scientific reports

Check for updates

OPEN

Control of work functions of nanophotonic components

Kanij Mehtanin Khabir, Mohammad Shahabuddin, Natalia Noginova & Mikhail A. Noginov✉

Work function is an essential material's property playing important roles in electronics, photovoltaics, and more recently, in nanophotonics. We have studied effects of organic, and inorganic dielectric materials on work functions of Au films in single layered, and multilayered structures. We found that measured work function of metallic surfaces can be affected by dielectric materials situated 10–100 nm away from the metallic surface. We have found that, (i) the glass underneath ~ 50 nm gold slab reduces the work function of gold, (ii) Rh590:PMMA increases the work function of a gold film deposited on top of the polymer, and (iii) reduces it if Rh590:PMMA is deposited on top of Au. (iv) With increase of the Rh590 concentration in PMMA, *n*, the work function first decreases (at *n* < 64 g/l), and then increases (at *n* > 64 g/l). (v) The work function of a Fabry–Perot cavity or an MIM waveguide is almost the same as that of single Au films of comparable thickness. The experimental results can be qualitatively explained in terms of a simple model taking into account adhesion of charged molecules to a metallic surface, and formation of a double layer of charges accelerating or decelerating electrons exiting the metal and decreasing or increasing the work function.

Light-Matter Interaction

Light-matter interaction (e.g., interaction of excitons with small cavities or surface plasmons) can occur in weak or strong coupling regimes[1–3].

In a weak coupling regime, the rates of energy relaxation, and dephasing exceed the rate of reversible exciton-cavity energy transfer[1,2]. (Here and below, we refer to a resonator as a "cavity", although surface plasmons will be discussed as well.) Weak coupling primarily affects the rates of spontaneous emission (e.g., Purcell effect[4]) but not the energy eigenstates of interacting constituents.

At the same time, in a strong coupling regime, the rate of the reversible energy transfer exceeds the relaxation rates, causing Rabi splitting $\hbar\Omega_R$ of the hybridized excited energy states[1],

$$\hbar\Omega_R = 2\sqrt{\frac{\hbar\omega}{2\varepsilon_0 v}}d\left(n_{ph}+1\right) \tag{1}$$

Where $\hbar\omega$ is the cavity resonance or transition energy, ε_0 the vacuum permittivity, v is the mode volume, d the transition dipole moment of the material, and n_{ph} the number of photons present in the mode. Furthermore, strong coupling affects both rates, and energies of the interacting states[1–3].

Strong coupling has been reported to influence emission[2], dispersion curves of surface plasmons and cavities[1–3,5], polariton condensation[6], spintronics[7], quantum information processing[8], electrical conductivity[9], rates of chemical reactions[10–13], and cavities' work functions[14]. The latter result is particularly intriguing as it suggests that work functions of metallic films can be affected by organic and inorganic molecules situated ~ 100 nm away from the metallic surface, in contrast to a common belief that electrons contributing to the work function measurements are located ~ 1 nm to ~ 3 nm below the surface[15] and in agreement with[14,16], where this characteristic length was 10 nm to 100 nm.

Work function

Fermi energy in metal, E_F, is the energy of the highest occupied electronic state (at 0 K). The gap in the energy spectrum between the Fermi level and the top of the energy scale at E = 0 (vacuum level) is called the work function ϕ[14,15,17,18]. The Fermi energy and correspondingly, the work function determine optical properties of metals (e.g., absorption loss)[19,20] which makes their fundamental studies and engineering particularly important. This motivated the present study of work functions in metal-dielectric structures described below.

Center for Materials Research, Norfolk State University, Norfolk, VA 23504, USA. ✉email: mnoginov@nsu.edu

Consider two metals with different work functions ϕ_1 and ϕ_2, Fig. 1a. If the two metals are brought in contact, electrons can lower the overall energy of the system by flowing from metal 1 to metal 2. They will continue until the two Fermi levels become the same. The consequence of this flow is an excess of electrons in one metal and a deficiency in the other, which can be observed as the potential difference between the two metals, known as contact potential. The contact potential is commonly represented by a spacing between the "$V = 0$" levels, Fig. 1b. The value of the contact potential is the difference between the two work functions[17].

Contact potential can be measured using a setup known as Kelvin Probe (KP), whose key component is a plane capacitor made of two metallic plates (M and N) with different work functions, Fig. 2a[17,21]. One of the plates (sample to be studied) stays still, while the second one (tip) vibrates in an oscillatory manner, driven by a motor. The latter oscillation of the effective capacitance causes sinusoidal current in the circuit, and the voltage at resistor r, which can be observed using an amplifier and an oscilloscope, Fig. 2a. An external potential can be applied to the plates and adjusted so that in continuous oscillation the voltage amplitude (V) is reduced to zero. The applied external potential is then equal to the contact potential, which is thus measured. The Kelvin Probe measures the difference, $\Delta\phi = \phi_s - \phi_{tip}$, between the work function of the sample to be studied, ϕ_s, and that of the tip, ϕ_{tip}. (We will omit subscripts where their usage is obvious.)

Measured work functions are highly sensitive to surface conditions, particularly the presence of an adsorbed surface layer of foreign atoms, as explained below. Consider an atom close to a metallic surface. If that atom has an easily removable electron that can join the metal at a lower energy than it had in an atom, a positive ion will be formed. Electrostatic attraction between the negatively charged metal surface and the positive ion will cause it to adhere to the surface. If a complete monoatomic layer of the ions covers the metal surface, a double sheet of charges will be formed, Fig. 2b.

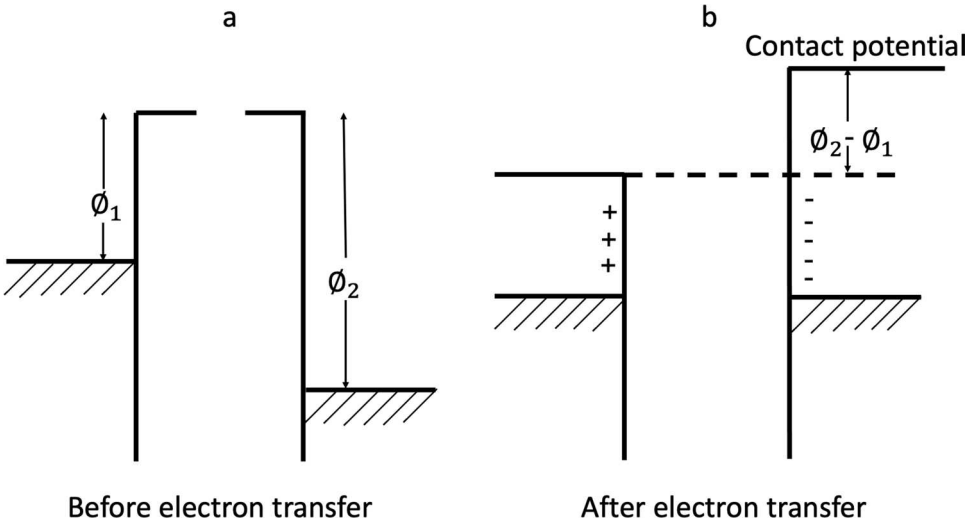

Figure 1. The Fermi levels and potentials of two metals (**a**) before; and (**b**) after the electron transfer, redraw from ref[17].

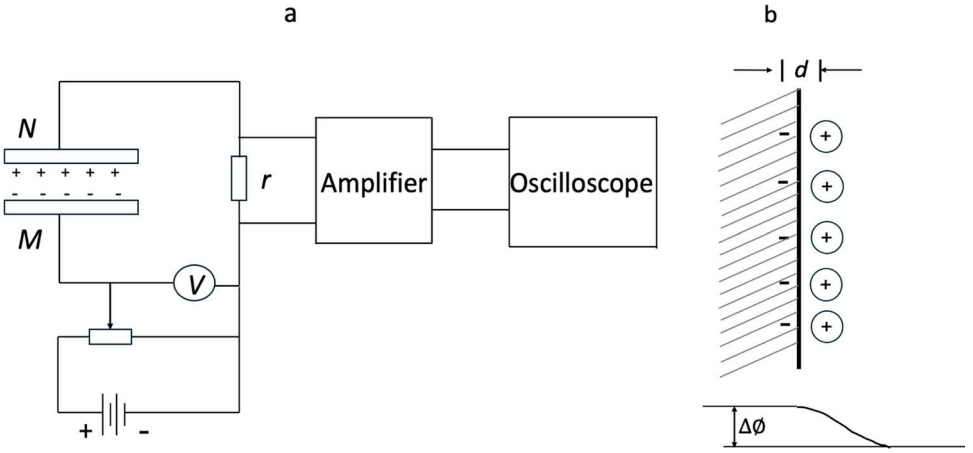

Figure 2. (**a**) Schematics of the Kelvin Probe apparatus redraw from ref[21]; (**b**) contribution to the work function of an adsorbed layer of atoms redraw from ref[17].

This gives rise to no external field, but there is a field in the space between two sheets of charges. Thus, if we extract an electron from inside the metal, the amount of work is reduced because of the assistance provided by this internal field in the surface layer. Therefore, a monoatomic layer of electropositive atoms reduces the work function of the surface. On the other hand, a layer of negative ions will increase the work function of the surface[17].

Strong coupling in electronic and photonic structures and materials

Important feature of strong coupling is that it occurs even in the absence of light: when n_{ph} in Eq. (1) goes to zero, $\hbar\Omega_R$ has a finite value. Thus, even in the dark, the interaction of the material with the vacuum field via the photonic structure can be very strong, comparable to $\hbar\Omega_R \sim 700$ meV demonstrated[12]. Such high values lead to a major reorganization of the energy levels of the system[13].

The authors[14] have explored whether strong coupling can be used to modify the work function (ϕ). They have demonstrated that the work functions of plasmonic hole arrays and Fabry–Perot cavities, characterized by the ~ 30–200 nm metal film dimensions, can be modified by engineering the electromagnetic environment of the material. It has been concluded that the measured change in the surface potential (SP) induced by strong coupling is due to a change in work function of the material. Furthermore, it was shown that the splitting of the excited state into upper $|P^+\rangle$ and low $|P^-\rangle$ polaritons does, indeed, affect the electronic energy levels.

Finally, the first non-optical observation of strong coupling[14] provides evidence that strongly coupled materials can be fundamentally modified even in the absence of light by the formation of new hybrid states. This further confirms the potential of strong coupling for materials engineering and device design.

In the present work, we have studied effects of organic and inorganic dielectric materials on work functions of Au films. We found that measured work functions of metallic surfaces can be affected by dielectric materials situated 10–100 nm away from the metallic surface, in agreement with[14] and disagreement with[15].

Experimental samples

Our experimental samples were single layered, double layered, and triple layered metallic films (Au and Al) and dye doped polymeric films (Rh590:PMMA) deposited on untreated (as is) glass slides. The photographs and AFM images of selected samples are depicted in Fig. 3 and several sample morphologies are shown in next section. Au films were deposited using the thermal evaporator (Nano 36 from Kurt J. Lesker). The thickness of metallic films, measured with DekTak XT stylus profilometer (from Bruker), ranged from 15 to 200 nm. The surface roughness of Au films (measured using Multiview 4000 AFM from Nanonics) was ~ 1.9 nm, Fig. 3b. The film's structure, depicted in Fig. 3b, is partly affected by the morphology of the substrate, e.g., glass or polymer.

In preparation of Rh590:PMMA films, PMMA and Rh590 were dissolved in dichloromethane, in ultrasonic bath at 24 °C for 60 min. The concentration of dye in solid state polymer (after solvent evaporated) ranged from 0 g/l to 1260 g/l (pure Rhodamine 590). Dye doped polymeric films were deposited using dip casting or drop casting (drop and dry) techniques. The thickness of the dye doped polymeric films ranged from 247 to 450 nm.

Samples were mounted on a metallic stage of the Kelvin Probe apparatus (from KP Technologies) and the electrical contact between the metallic film and the stage was provided by an adhesive copper tape.

Work function measurements

Control measurement

In the first control experiment, the 215 nm Au film and the 115 nm Al film were deposited side by side onto a glass substrate, Fig. 4. The work function of the tip ϕ_{tip} (Au-based alloy) was found to be smaller than that of Au, $\phi_{tip} < \phi_{Au}$, and larger than that of Al, $\phi_{tip} > \phi_{Al}$, resulting in the difference between the work functions of Au and Al equal to $\phi_{Au} - \phi_{Al} = 820$ meV. The latter value is consistent with those reported in the literature for bulk metals[22]. (The positive sign means that in the schematics of Fig. 2a, the Fermi level in Au is lower than that in Al). Thus, ~ 100–200 nm Au and Al films can be treated as bulk, and thickness dependence of their work functions can be neglected. (The situation becomes different when metallic films are thin).

In the second control experiment, Au and Al films were deposited to partly overlap each other, Fig. 5. The "pure Au" and "pure Al" sections of the films had work functions expectedly similar to those found in the previous experiment, while the work function of the overlapped segment was identical to that of pure gold. The outcome of this experiment can be different in thinner Au films. This is the topic of the future study to be published elsewhere.

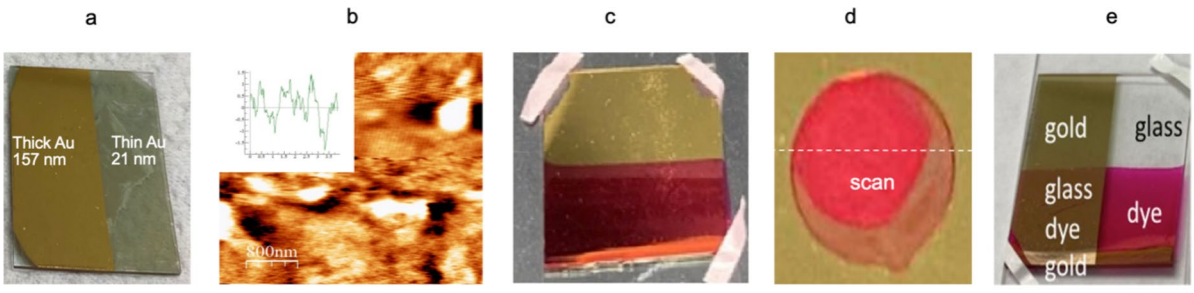

Figure 3. (**a**) Au films of different thickness deposited on glass; (**b**) AFM scan and surface profile of Au film; (**c**) dip cast dye doped polymer on top of Au; (**d**) drop cast dye doped polymer film on top of Au; and (**e**) Au on top of dye.

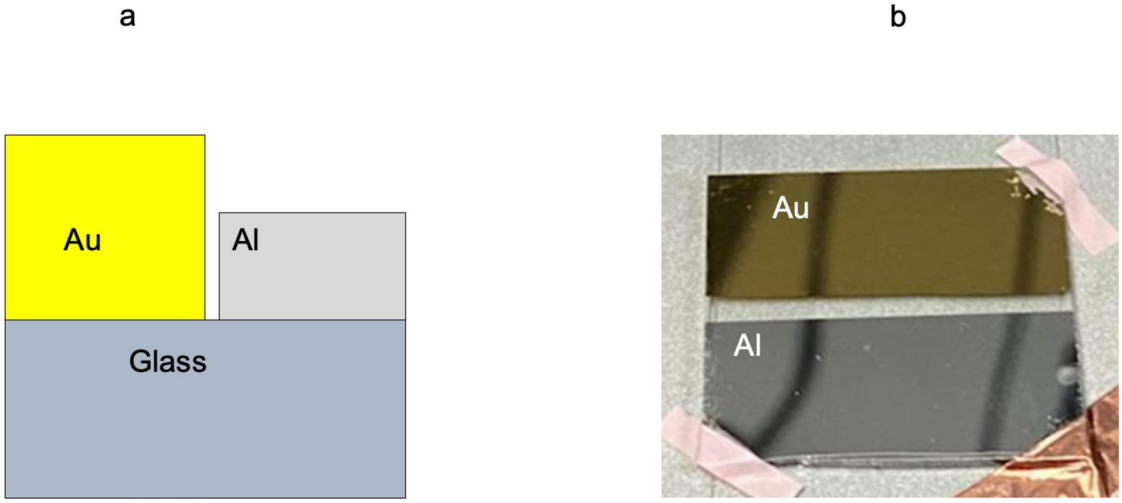

Figure 4. Au and Al films on glass: (**a**) morphology; and (**b**) photograph.

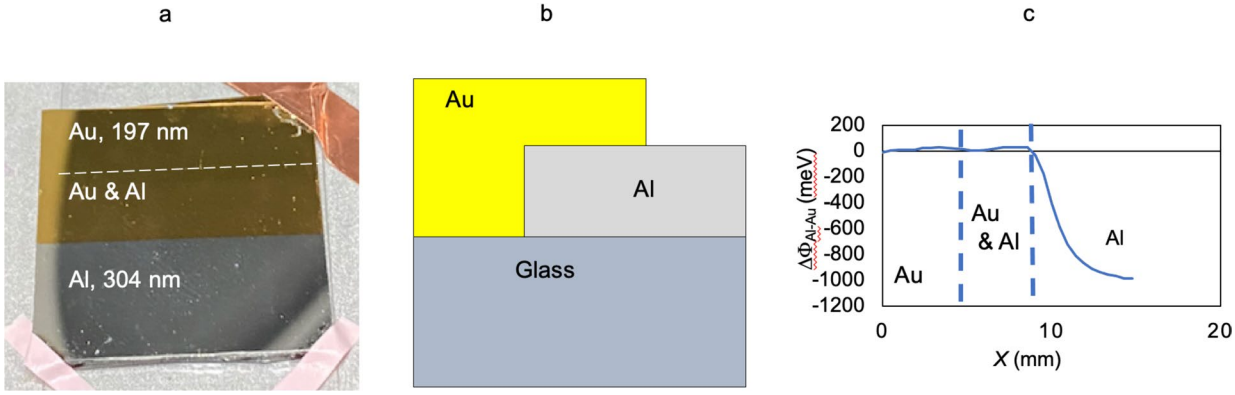

Figure 5. (**a**) Photograph; (**b**) morphology of the sample with overlapped Au and Al layers; and (**c**) work functions in pure Au (left), pure Aluminum (right) and Au and Al (central) samples. *X* is the lateral position of the Kelvin Probe tip.

Gold films of different thickness deposited on glass

In the two experiments described below, we have studied the work functions in Au films of different thickness deposited on glass.

In the first particular experiment, we deposited Au films onto four glass slides. One half of each film was thin (21 nm, 35 nm, 50 nm, and 79 nm), and the other half was thick (157 nm, 178 nm, 192 nm, and 203 nm, respectively), Fig. 6a and b. In all samples we measured the work functions of thin and thick Au films and found them to be substantially different from each other, Fig. 6c. Their difference $\phi_{thick} - \phi_{thin}$, is plotted as a function of

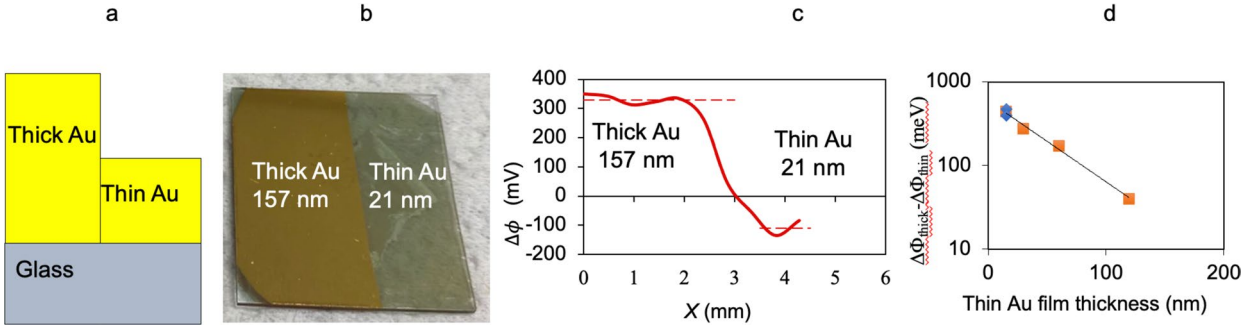

Figure 6. Thick and thin Au films on a glass substrate: (**a**) morphology; (**b**) photograph; (**c**) ϕ_{Au}-ϕ_{tip} measured on thick (157 nm) and thin (21 nm) halves of the Au film; and (**d**) $\phi_{thick} - \phi_{thin}$ measured in thick and thin halves of Au films, plotted against the thickness of thin halves *d*. *X* is the lateral position of the Kelvin Probe tip.

the thickness d of the thin half of the Au film, Fig. 6d. Intriguingly, $\phi_{thick} - \phi_{thin}$ drops exponentially as a function of d, with the characteristic "skin depth" equal to 45 nm, Fig. 6d.

In the next particular experiment, we deposited four Au films of different thicknesses d (17 nm, 30 nm, 59 nm, and 100 nm) onto a glass substrate and measured their work functions relative to that of the tip, $\Delta\phi = \phi_{Au} - \phi_{tip}$. As one can see in Fig. 7, $\Delta\phi$ becomes smaller with reduction of d (reduction of the work function with the reduction of the film's thickness) in agreement with the previous experiment. (We want to emphasize that in this particular experiment, we studied the films work functions measured relative to the tip, while in the previous experiment, we analyzed the difference between the work functions in thick and thin films.)

To summarize two last experiments, with the reduction of the Au film thickness, its work function drops, supposedly, from that of bulk Au to a much smaller value ($\Delta\phi > 0.5$ eV), with the characteristic "skin depth" equal to 45 nm.

Control of Au work function with a dye-doped polymer

In the three experiments described below, we studied the effect of dye-doped polymer (Rh590:PMMA) on the Au work function.

In the first experiment of this series, we deposited Rh590:PMMA films (n = 512 g/l) of different thickness l onto Au films, whose thickness ranged between d = 160 nm, and d = 226 nm in Fig. 8a,b, and observed a dramatic reduction of the work function of coated Au (measured relative to the tip, $\Delta\phi = \phi_{Au} - \phi_{tip}$), Fig. 8c. The dependence of the work function on the thickness of the Rh590:PMMA films, $\Delta\phi_{cp}(l) = \phi_{coated} - \phi_{pristine}$, was modest at small l and practically nonexistent at large l. Interestingly, the dependence $\Delta\phi_{cp}(l)$ was linear if plotted versus $\ln(l)$ (logarithmic dependence), Fig. 8d.

In the second particular experiment, the dye concentration in PMMA was also equal to 512 g/l. The dye-doped films of thickness l ranging from 206 to 281 nm were deposited on Au films, whose thickness d was equal to 19 nm, 34 nm, 59 nm, and 109 nm, were deposited on top of Rh590:PMMA, Fig. 9a,b. The corresponding work functions, measured relative to the tip, were larger in Au films deposited on top of Rh590:PMMA than those in pristine Au films, Fig. 9c. This result is directly opposite to the one reported in the experiment described above (Au on top of R6G:PMMA). The larger difference was found in the samples with thin Au films and the latter difference decreased with the increase of d. When the difference of the work functions on top of Rh590:PMMA and on top of pristine Au was plotted versus d, the resultant dependence could be fitted with the exponent whose skin depth is equal to 130 nm, Fig. 9d.

The purpose of the next particular experiment was to study the dependence of the work function on the concentration of Rh590 dye in PMMA. To achieve this goal, Rh590:PMMA solutions with Rh590 concentrations ranging from 0 g/l (pure PMMA) to 1260 g/l (pure Rh590) have been prepared and drop cast on top of ≈ 200 nm Au films, Fig. 10a,b. The thickness of Rh590:PMMA films was ≈ 200 nm. Similarly, to the first experiment of this series, polymeric films significantly (up to 700 meV) reduced the work functions (measured relative to the

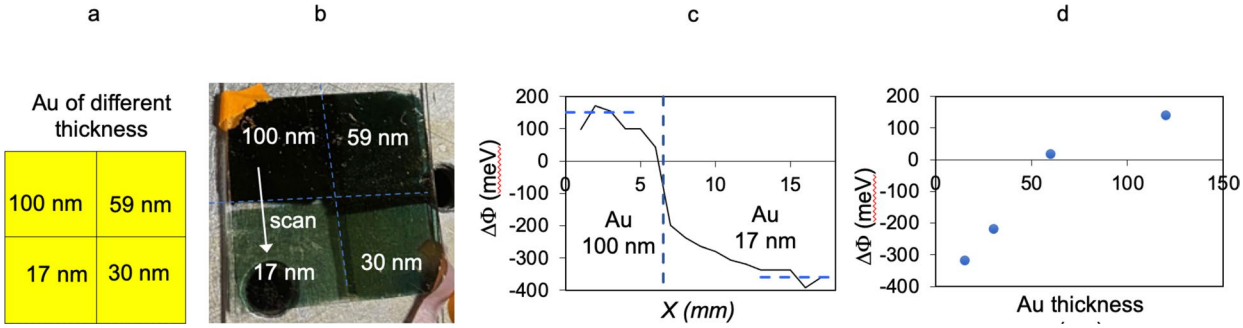

Figure 7. Four segments of Au film on a glass substrate: (**a**) morphology (top view); (**b**) photograph; (**c**) $\phi_{Au} - \phi_{tip}$. measured on thick (100 nm), and thin (17 nm) quarters of the Au film; and (**d**) ϕ_{thick}- ϕ_{thin} measured as the function of Au thickness.

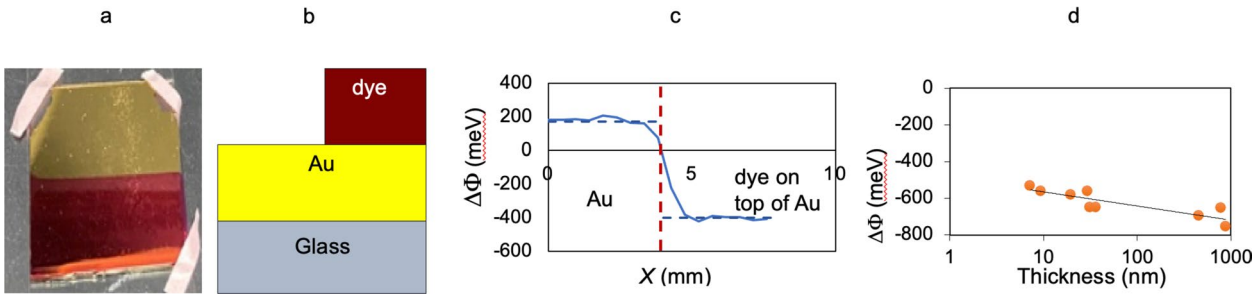

Figure 8. Pristine and Rh590:PMMA coated Au film on a glass substrate: (**a**) photograph (top view); and (**b**) morphology (side view); (**c**) $\Delta\phi = \phi_{Au} - \phi_{tip}$ measured in pristine Au (left) and polymer-coated (right) halves of the film; and (**d**) $\Delta\phi_{cp} = \phi_{coated} - \phi_{pristine}$ plotted as the function of the polymer thickness l.

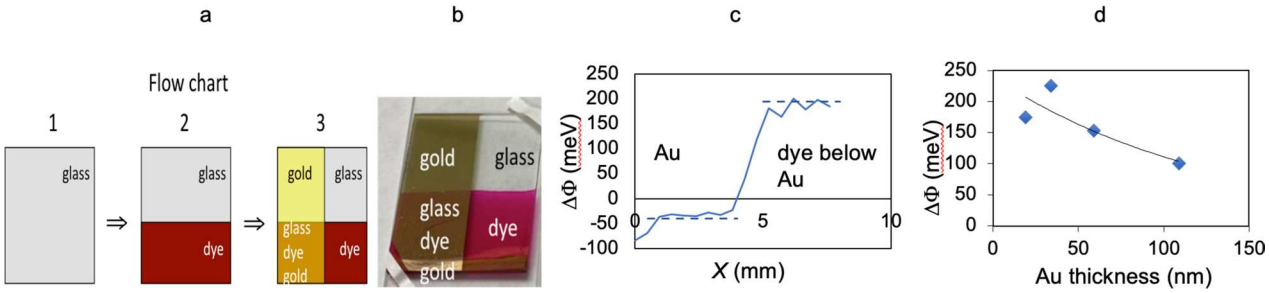

Figure 9. Au on top of Rh590:PMMA deposited on a glass substrate: (**a**) morphology and flow chart (top view); (**b**) photograph (top view); (**c**) $\Delta\phi = \phi_{Au} - \phi_{tip}$ measured in pristine Au (left) and polymer-coated (right) halves of the sample; and (**d**) $\Delta\phi_{cp} = \phi_{coated} - \phi_{pristine}$ as function of the thickness d of Au films.

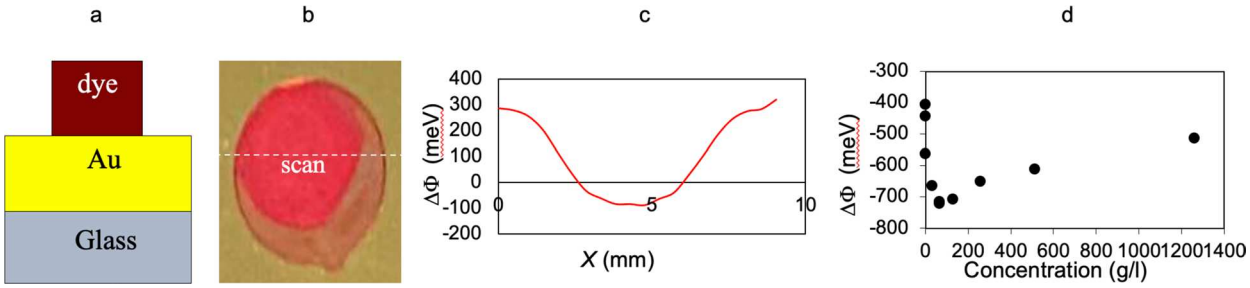

Figure 10. Dependence of the work function on concentration of Rh590: (**a**) morphology (side view); and (**b**) photograph (top view); (**c**) $\Delta\phi = \phi_{Au} - \phi_{tip}$ measured in pristine Au (left and right) and polymer-coated (center) parts of the sample; and (**d**) $\Delta\phi_{cp} = \phi_{coated} - \phi_{pristine}$ measured at different concentrations of Rh590 in PMMA.

tip, Fig. 10c) in comparison to those in pristine Au, Fig. 10. The dependence of $\Delta\phi_{cp} = \phi_{coated} - \phi_{pristine}$ on the dye concentration n was strong at small values n; it reached the minimal negative value at n ≈ 64 g/l, after which $\Delta\phi_{cp}$ slowly increased toward zero, Fig. 10d. In accord with the first experiment of this series, we did not observe any significant dependence of $\Delta\phi$ on the Rh590:PMMA film thickness.

Work functions in multi-layered samples

In the next particular experiment, we studied the work functions of Fabry–Perot cavities or Metal–Insulator-Metal (MIM) waveguides. The dye concentration in PMMA was 512 g/l, and the cavity sizes (thicknesses of the Rh590:PMMA layers) were equal to 50 nm, 110 nm, and 200 nm. The cavities of these sizes demonstrated strong coupling with the semiconducting polymer P3HT[11], whose absorption band was close to that of Rh590[23].

We first deposited Au film (200 nm) onto half of the glass slide in the "longitudinal" direction, Fig. 11a. Second, we deposited Rh590:PMMA film (via dip casting) in the "transversal" direction, covering half of the Au film and half of the not coated glass, Fig. 11a. Finally, we deposited 50 nm Au layer onto the dye-doped film, which was situated above the bottom Au film, forming a cavity, Fig. 11a,b. Thus, within one sample, we created four areas suitable for the Kelvin Probe measurements: Segment 1—pristine Au, Segment 2—cavity, Segment 3—Au on top of dye, and Segment 4—dye on top of Au. Two other Segments were Rh590:PMMA on glass and uncoated glass.

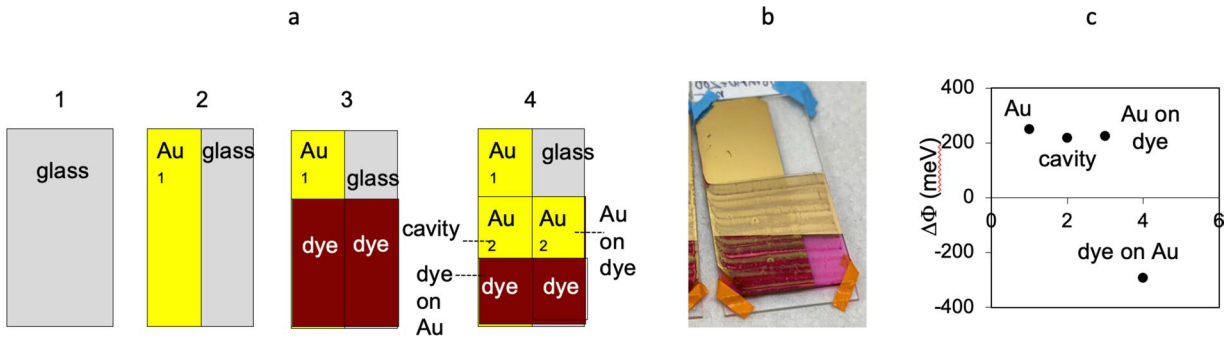

Figure 11. Work functions in multi-segment structures: (**a**) morphology/flow chart (top view); (**b**) photograph (top view); $\Delta\phi = \phi_{Au} - \phi_{tip}$ measured in pristine Au (Segment 1), cavity (Segment 2), Au on top of Rh590:PMMA (Segment 3), and Rh590:PMMA on top of Au (Segment 4); (**c**) averaged over six measurements.

The electrical resistance measured between two points in the bottom Au layer (separated by 1 cm) was equal to 0.8 Ω. At the same time, the resistance measured between the top and the bottom Au layers, across the dye doped PMMA layer, was approximately equal to 6 Ω. The latter value did not change significantly (within factor of two) with the change of the thickness of the Rh590:PMMA layer or the dye concentration. This result is surprising because the resistivity of PMMA is very high[24] and the expected conductance is equal to 2×10^{13} Ω. This discrepancy is possibly due to the fact that the PMMA layer had voids resulting in a short circuit electrically connecting two Au films.

We measured the work functions in six multi-segmented samples: thickness of Rh590:PMMA = 50 nm, 110 nm, and 200 nm, with and without intentional short circuit connection between the top and the bottom Au films. The electrical conduit was attached to Segment 1 (Au film in the bottom). We found that within the experimental error, the work functions of pristine Au (Segment 1), cavity (Segment 2), and Au on top of Rh590:PMMA (Segment 3) were almost equal to each other, Fig. 11c. The equivalence of the work functions in Segments 1 and 3 is particularly surprising since the work functions of pristine Au and Au on top of Rh590:PMMA were strongly different from each other in simpler sample configurations, Fig. 9 (Au = 35 nm). The strong reduction of the work function in Au films covered with the dye-doped polymer (Segment 4), in comparison with that of Au (Segment 1), was in agreement with the one depicted in Fig. 8.

Note that the work function was marginally larger when (i) the electrical conduit was attached to Segment 3 (Au on top of Rh590: PMMA) rather than Segment 1 (pristine Au), and (ii) when no intentional short circuit connection had been made. Figure 11c depicts the average values of the work functions measured in samples with 50 nm, 110 nm and 200 nm thick dye-doped PMMA film.

Discussion

As it has been discussed in Sect. "Light-Matter Interaction", adhesion of a layer of positively charged atoms to a metallic surface causes formation of a double sheet of charges that accelerate electrons exiting the metal to the right, and reducing the corresponding work function, Fig. 2b. This qualitative reasoning remains true if the size of the double sheet of charges is comparable to the thickness of the metallic sheet d, Fig. 12a. This is, arguably, the case of (positively charged) Rh590:PMMA on top of Au in our experiment.

If positively charged molecules are adhered to the left wall of the metallic slab, the double layer of charges increases the work function for electrons exiting the slab to the right, Fig. 12b. This is likely the case of Au deposited on top of Rh590:PMMA.

If negatively charged molecules forming glass are adhered to the left wall of the metallic slab, the double layer of charges reduces the work function for electrons exiting the slab to the right, Fig. 12c. This is probably the case of Au deposited on top of glass. (This effect is possible when the thickness of Au film is not very large, comparable to the thickness of the double layer.)

Structures of Fig. 12a,b, brought together, form a metal–insulator-metal (MIM) waveguide or a Fabry–Perot cavity, Fig. 12d. As one of the constituent structures causes the reduction of the work function, while the second one causes its increase, one can hypothesize that the combination of these two structures (forming a cavity) will have a very small (if any) effect on the overall cavity's work function. This result is in qualitative agreement with the experiment of Section "Strong coupling in electronic and photonic structures and materials".

Thus, despite of multiple assumptions and simplifications, such as omission of the glass substrate in the schematics depicted in Fig. 12a,b,d, the hand-waiving model presented in this Section qualitatively explains experimental behavior of work functions in various nanophotonic environments.

The other assumptions were "long action" of the measured work function and favorable relationship between the "skin depth" of the work function and the thickness of the metallic slabs. These effects as well samples' inhomogeneity and Van Der Waals interactions are the subject of the future studies to be published elsewhere.

Summary

Work function is an important material's property playing important roles in electronics, photovoltaics, and more recently, nanophotonics. At this time, we have studied effects of organic (Rh590:PMMA), and inorganic (glass) dielectric materials on work functions of Au films. We have found that the measured work function of a metallic surface can be affected by a dielectric material situated 10–100 nm away from the surface.

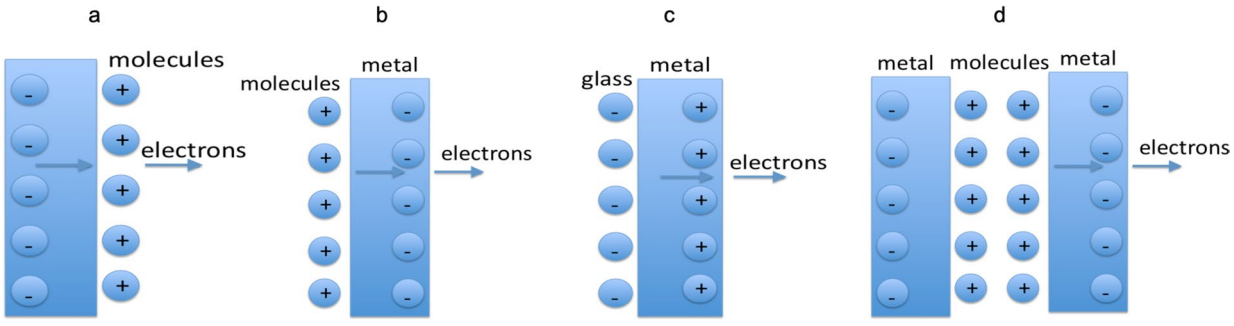

Figure 12. Sample morphologies discussed here.

Our samples were single-layered, double-layered, and triple-layered Au and Rh590:PMMA films deposited on glass. We have found that glass reduces the work functions of Au surfaces separated from glass by ~ 50 nm gold slabs.

On the contrary, Rh590:PMMA increases the work function of a Au film deposited on top of Rh590:PMMA, and reduces it if Rh590:PMMA is deposited on top of Au.

With increase of the Rh590 concentration in PMMA, the work function first decreases (at $n < 64$ g/l), and then increases (at $n > 64$ g/l).

The work function of a Fabry–Perot cavity or an MIM waveguide is almost the same as that of relatively thick Au films.

The experimentally observed experimental behavior can be qualitatively explained in terms of a simple model taking into account adhesion of charged molecules to a metallic surface, formation of a double layer of charges accelerating or decelerating electrons exiting the metal, and correspondingly, decreasing or increasing the work function.

Data availability

The datasets used and/or analysed during the current study available from the corresponding author on reasonable request.

Received: 14 November 2023; Accepted: 26 July 2024
Published online: 05 August 2024

References

1. Törmä, P. & Barnes, W. L. Strong coupling between surface plasmon polaritons and emitters: A review. *Rep. Prog. Phys.* **78**(1), 013901 (2014).
2. Ebbesen, T. W. Hybrid light–matter states in a molecular and material science perspective. *Acc. Chem. Res.* **49**(11), 2403–2412 (2016).
3. Lidzey, D. G. & Coles, D. M. Strong Coupling in Organic and Hybrid-Semiconductor Microcavity Structures. In *Organic and Hybrid Photonic Crystals* (ed. Comoretto, D.) (Springer, Cham, 2015). https://doi.org/10.1007/978-3-319-16580-6_11.
4. Purcell, E. M. Spontaneous emission probabilities at radio frequencies. *Phys. Rev.* **69**, 681 (1946).
5. Zhang, K. *et al.* Couple molecular excitons to surface plasmon polaritons in an organic-dye-doped nanostructured cavity. *Appl. Phys. Lett.* **108**, 193111 (2016).
6. Byrnes, T., Kim, N. Y. & Yamamoto, Y. Exciton–polariton condensates. *Nat. Phys.* **10**(11), 803–813 (2014).
7. Rocha, A. *et al.* Towards molecular spintronics. *Nat. Mater.* **4**, 335–339. https://doi.org/10.1038/nmat1349 (2005).
8. Reithmaier, J. *et al.* Strong coupling in a single quantum dot–semiconductor microcavity system. *Nature* **432**, 197–200 (2004).
9. Orgiu, E. *et al.* Conductivity in organic semiconductors hybridized with the vacuum field. *Nat. Mater.* **14**, 1123–1129 (2015).
10. Peters, V. N., Tumkur, T. U., Zhu, G. & Noginov, M. A. Control of a chemical reaction (photodegradation of the P3HT polymer) with nonlocal dielectric environments. *Sci. Rep.* **5**, 14620 (2015).
11. Peters, V. N. *et al.* Effect of strong coupling on photodegradation of the semiconducting polymer P3HT. *Optica* **6**(3), 318–325 (2019).
12. Schwartz, T., Hutchison, J. A., Genet, C. & Ebbesen, T. W. Reversible switching of ultrastrong light-molecule coupling. *Phys. Rev. Lett.* **106**, 196405 (2011).
13. Hutchison, J. A., Schwartz, T., Genet, C., Devaux, E. & Ebbesen, T. W. Modifying chemical landscapes by coupling to vacuum fields. *Angew. Chem.* **51**, 1592–1596 (2012).
14. Hutchison, J. A. *et al.* Tuning the work-function via strong coupling. *Adv. Mater.* **25**, 2481–2485 (2013).
15. Ambient Pressure Photoemission Spectroscopy System Manual: For Software Series 12 and Hardware Version APS04, KP Technology, *APS manual* (2018).
16. Ravi, S. K., Sun, W., Nandakumar, D. K., Zhang, Y. & Tan, S. C. Optical manipulation of work function contrasts on metal thin films. *Sci. Adv.* **4**(3), eaao6050 (2018).
17. T. S. Hutchison, and D. C. Baird, "The Physics of Engineering Solids," John Wiley, and Sons, Inc., New York, London, Sydney, second edition, 534 (1968).
18. Baikie, I. D. & Estrup, P. J. Lowcost PC based scanning Kelvin probe. *Rev. Sci. Instrum.* **69**(11), 3902–3907 (1998).
19. Potter, K. S. & Simmons, J. H. *Optical materials* 530 (Elsevier, 2021).
20. Bobb, D. A. *et al.* Engineering of low-loss metal for nanoplasmonic and metamaterials applications. *Appl. Phys. Lett.* **95**, 151102 (2009).
21. Sivukhin, D.V. Obshii kurs fiziki. Tom 3: Elektrichestvo. Izdanie 2-E, Ispravlennoe, *IZD-VO NAUKA*, Moskva, pp **688** (1983), in Russian.
22. Denker, J. Work functions (2012). www.av8n.com/physics/workfun.htm
23. Chowdhury, M. G., Hesami, L., Howard, S. & Noginov, M. A. *Anomalous Dispersion of Strongly Coupled Surface Plasmon Polaritons and Dye Molecules* 2–39 (CLEO Fundamental Science, Optica Publishing Group, 2023).
24. Shaari, H. A. H., Ramli, M. M., Mohtar, M. N., Rahman, N. A. & Ahmad, A. Synthesis and conductivity studies of poly (Methyl Methacrylate) (PMMA) by co-polymerization and blending with polyaniline (PANi). *Polymers* **12**(13), 1939 (2021).

Acknowledgements

This work was supported by NSF Grants 1830886, 1856515, 2112595, and 2301350, DOE awards DE-NA0004007 and DE-NA-0003525.

Author contributions

M.A.N. designed the study of the work function measurements of different type of samples. K.M.K. accomplished the whole experiments. K.M.K. and M.A.N. executed the data analysis of all measurements. M.S contributed to operate the KP machine. N.N. contributed to sample fabrication. K.M.K and M.A.N prepared the figures. K.M.K. and M.A.N. wrote the manuscript.

Competing interests

The authors declare no competing interests.

Additional information

Correspondence and requests for materials should be addressed to M.A.N.

Reprints and permissions information is available at www.nature.com/reprints.

Publisher's note Springer Nature remains neutral with regard to jurisdictional claims in published maps and institutional affiliations.

Open Access This article is licensed under a Creative Commons Attribution-NonCommercial-NoDerivatives 4.0 International License, which permits any non-commercial use, sharing, distribution and reproduction in any medium or format, as long as you give appropriate credit to the original author(s) and the source, provide a link to the Creative Commons licence, and indicate if you modified the licensed material. You do not have permission under this licence to share adapted material derived from this article or parts of it. The images or other third party material in this article are included in the article's Creative Commons licence, unless indicated otherwise in a credit line to the material. If material is not included in the article's Creative Commons licence and your intended use is not permitted by statutory regulation or exceeds the permitted use, you will need to obtain permission directly from the copyright holder. To view a copy of this licence, visit http://creativecommons.org/licenses/by-nc-nd/4.0/.

© The Author(s) 2024